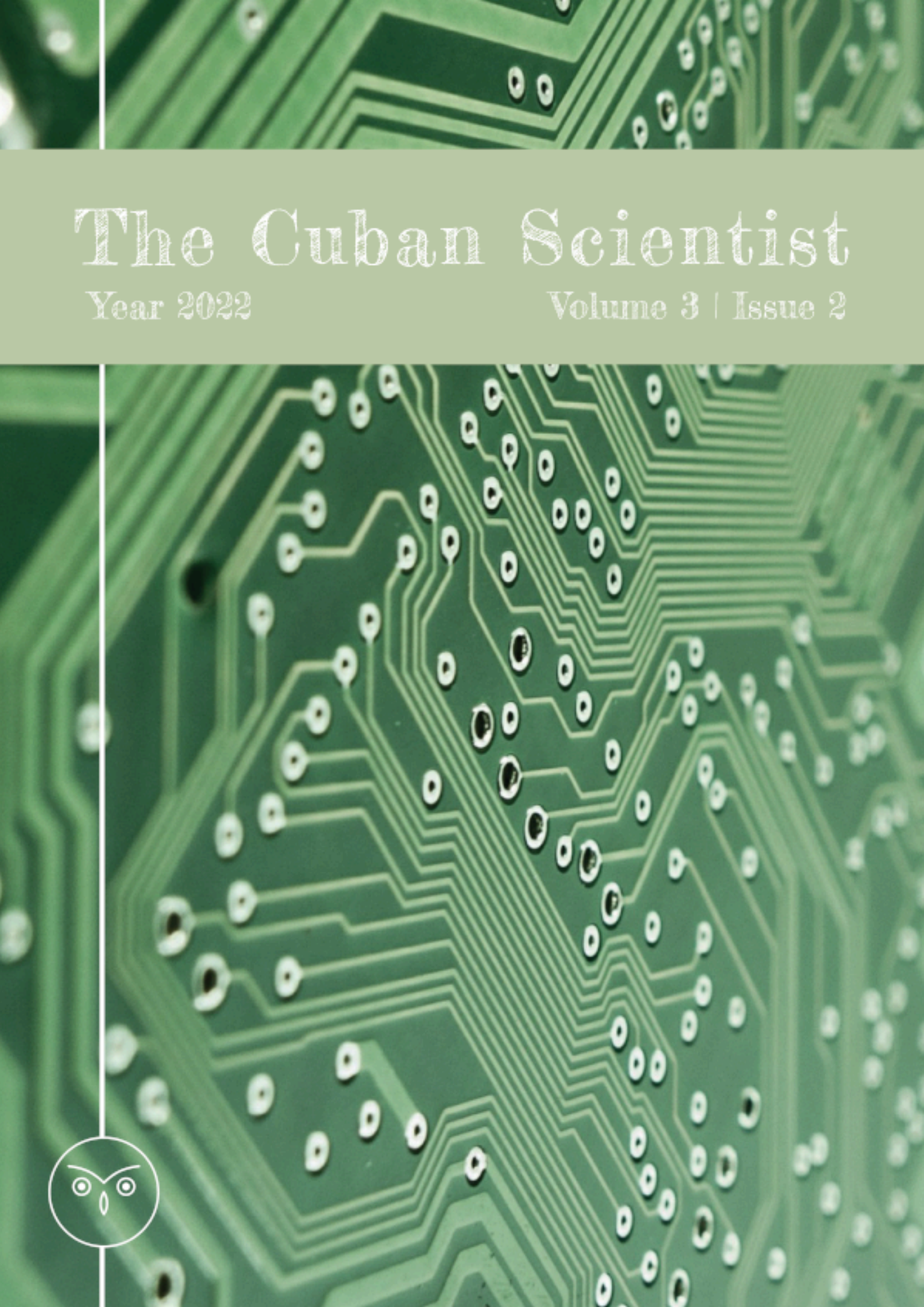

The Cuban Scientist

Year 2022

Volume 3 | Issue 2

In this issue:

The historiography of pictorial art in 19th century colonial Cuba

Osvaldo Paneque Duquesne[a1]

[1]Faculty of Arts and Letters. University of Havana

We introduce to the representative texts on the historiography of pictorial art in 19th century, and the history they reveal, using descriptive statistical analysis to gain a quantitative understanding of the set.[b]

Introduction

Current studies on academic colonial painting produced in Cuba present a better picture than in previous years. The National Museum of Fine Arts and the Faculty of Arts and Letters of the University of Havana, among others, have contributed to this. There are some periodisations and articles that attempt to give a historical account of the development of painting during the period in question, but they are still insufficient for a broad and detailed knowledge of the subject. There is a need for studies that would make it possible to delve more deeply into certain thematic areas, time periods or artists, which could make up for the shortcomings that still persist.

The vision of academic painting produced in Cuba has been shaped, fundamentally, on the basis of the criteria of the authoritative voices on the subject that circulate in texts (books, catalogues, periodicals, etc.). The aim of this paper is therefore to explain which are the most representative texts and what is the history they reveal.

We present writings on art that refer to academic colonial painting, its artists and the contexts in which they developed. We do not intend at this point to make a totalising analysis, for that it will be necessary to combine historiographic visions with the analysis of works and collections. In addition, an exposition of the dissimilar meanings of historiography is given. We also look at some of the characteristics of Cuban historiography in its three historical periods (Colony, Republic, Revolution).

All of the above is done in order to place the art historiography, the starting point of our study, on a solid foundation. This is where these texts on academic colonial painting will be found, marked by the characteristics of the historiography of each period.

Finally, the statistical results of the set of texts dealt with in this work can be observed in order to obtain the quantitative description and composition of this historiographical sample. This means that future analyses will have at their disposal a wide range of writings with certain characteristics that allow for a historiographical type of research in which diachronic and synchronic views can be combined.

Development

The distribution of the texts observed can be seen in figure 1, where the variability of media is appreciable, with the highest percentage belonging to scientific articles and books.

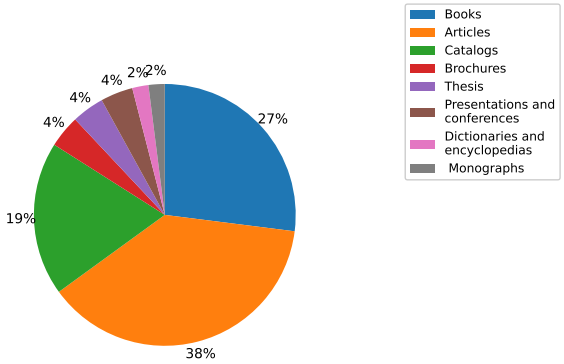

Figure 1: Composition of the texts under study according to their type.

Similarly, the distribution of texts by country is shown in figure 2. Note that the highest percentage (74%) belongs to texts published in Cuba and that their variability allows us to contrast the views on academic colonial painting produced in Cuba by authors from various parts of the world, where Spanish and American texts predominate after the Cuban ones.

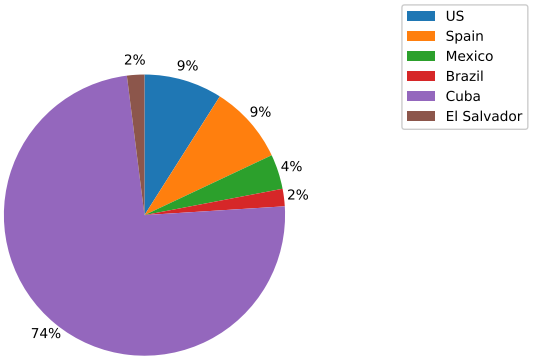

Figure 2: Composition of the texts that make up the object of study.

Figure 3 shows how the selection of these texts is composed according to the period to which they be-

long. Table 1 shows how the selected texts cover the three periods of Cuban history, as well as the variation within the same period. It should be noted that there are texts that are repeated in the same year; however, the intention is to show the variability and not the quantity.

Colony	Republic	Revolution			
1861	1924	1959	1983	2001	2013
1875	1936	1970	1986	2004	2016
1878	1947	1974	1990	2008	2017
1887	1950	1976	1991	2009	2018
1891	1952	1980	1994	2010	
	1953	1982	2000	2012	

Table 1: Distribution of texts by period and by year.

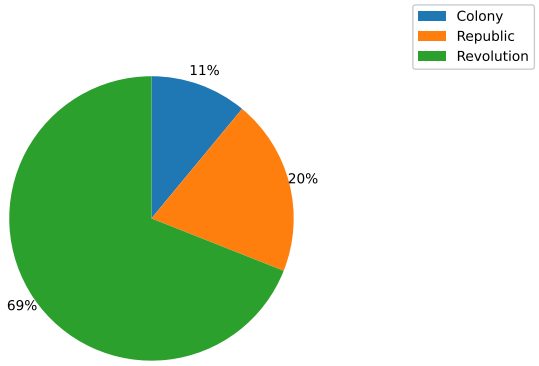

Figure 3: Distribution of the texts according to the period of Cuban history to which they belong.

Conclusions

The selection of texts presented here leads us to affirm that there is a propitious working scenario for investigating and continuing to construct the view of academic colonial painting produced in Cuba from other visions and inputs. What has been presented in this review invites researchers to consider other perspectives on the pictorial art produced in Cuba under the norms established by the Academy of San Alejandro.

It highlights the growing interest of the scientific and academic community to investigate, using the historiographic method, the relationship between the Academy of San Alejandro and its enabling context. This leads to the conclusion that the historiography carried out so far on the emergence and development of San Alejandro in the 19th century and the aspects surrounding it (painters, pupils, teachers, works) is, however, still scarce.

From the above, it is clear that it is necessary to combine not only the synchronic and diachronic aspects, but also the contextual aspects in which each of the texts cited here were written, as well as the fieldwork in the archives.

The aim of this study was to identify, even quantitatively, the elements from which future research into the academic painting of the colonial period in Cuba could be nourished.

For the Cuban colonial period, the texts presented meet certain requirements that will also make it possible to establish different approaches according to the socio-economic, social, cultural, geographical and political environments of the authors and their historiographical works.

The importance of taking up the issues raised in the works presented, the problematisation they propose, and the approach they provide, as well as the methodological processes they use, will lead to the development of more integrative proposals in future research. This is precisely the space that this historiographical exhibition is intended to establish, which obviously has the common denominator of the development of painting in Cuba, and among this the one with an academic character.

It should be remembered that the approach presented here does not have a totalising character, as the elements proposed by these authors require more in-depth work in which information is collated between the data provided by these authors, the documents present in the official archives and the texts describing the context of Cuba in the 19th century.

Notes

a. Email: osvaldo.paneque@gmail.com

b. Original version of this article is in Ref [1]

References

[1] Duquesne, O. P., La historiografía sobre el arte pictórico en la Cuba colonial del siglo XIX, *Nexus,* **28** (2020) 1-30.

Dark matter constraints from dwarf galaxies: a data-driven analysis

Bryan Zaldívar [a1]

[1]Institute of Corpuscular Physics, University of Valencia and CSIC, Spain

The dwarf satellite galaxies of the Milky Way are ideal targets to search for non-gravitational interactions of dark matter using gamma-ray data. A new data-driven method is proposed to bypass the currently limited knowledge of the physics behind standard astrophysical emissions.

Dark matter (DM) constitutes about 27% of the matter-energy content of our Universe and discovering its nature is one of the biggest challenges of contemporary physics. In the leading paradigm, DM is a new particle, beyond the framework of the standard model for particle physics. Several candidates in different ranges of mass and interaction strength exist and can account for the purely gravitational DM observational evidence. One of the most promising class of candidates are weakly interacting massive particles (WIMPs), which can naturally account for the observed DM cosmological relic density with annihilation cross section $\langle \sigma v \rangle$ around the benchmark value of 3×10^{-26} cm^3/s. Via their residual annihilations today, these DM particle candidates can produce stable particles such as photons and charged cosmic rays as a consequence of decay and hadronisation of the final states (quarks, gauge bosons, leptons, higgses), see Fig. 1. The ensuing signal can, in principle, be detected by space- and ground-based telescopes. However, this possibility is challenged by the typically dominant astrophysical emissions, which one has to disentangle a WIMP signal from. Among the best channels to look for DM is the high energy gamma-rays, from hundreds of MeV up to TeV energies. One of the most promising targets are dwarf spheroidal galaxies (dSphs), satellites of the Milky Way located within a few hundreds kiloparsec from the Galactic centre and whose mass is dominated by DM, as inferred from the kinematics of their stars. With little intrinsic astrophysical background emission expected, dSphs could be shining in gamma rays mostly in reason of their DM content, through annihilation (or decay) of WIMP particles.

The leading experiment measuring GeV-to-TeV gamma-ray data from the whole sky, including dSphs, is the Large Area Telescope, aboard the Fermi satellite (hereafter, Fermi-LAT) from the NASA, see Fig. 2. The Fermi collaboration models the standard astrophysical diffuse emission of gamma-rays as a linear combination of spatial "templates" including different physical components, as the neutral hydrogen as well as CO interstellar gas, inverse compton scattering, plus a modelling of the emission from large-scale structures as the so-called "Fermi-bubbles", extragalactic isotropic emission, and finally cataloged point-like sources. Such modelling has several limitations though, one of the most important ones being its incapability to account for a spatially-dependent unresolved population of unknown astrophysical objects. In addition to that, it is unclear how to determine in a sound way the uncertainties associated to the expected astrophysical emission from these templates.

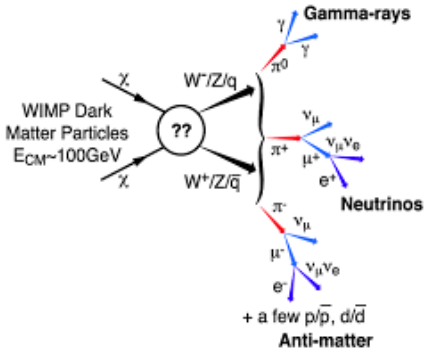

Figure 1: Pair annihilation of DM particles χ into different possible Standard Model particles. Fig. taken from the Fermi-LAT collaboration, fermi.gsfc.nasa.gov.

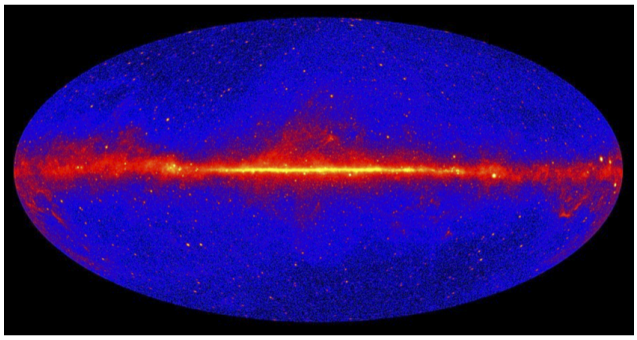

Figure 2: All-sky gamma-ray map produced by Fermi-LAT using 9 years of data collected from 2008 to 2017. See fermi.gsfc.nasa.gov.

In the context of DM searches, the above astrophysical emissions constitute the background against which to extract a potential DM signal, the latter representing the physics of interest. In this sense, the background emission can be thought (in a statistical jargon) as a "nuisance contribution". The idea, first presented in Ref. [1], is then to model the background emission using Machine Learning (ML) techniques, in a purely data-driven way, agnostic to the physics gov-

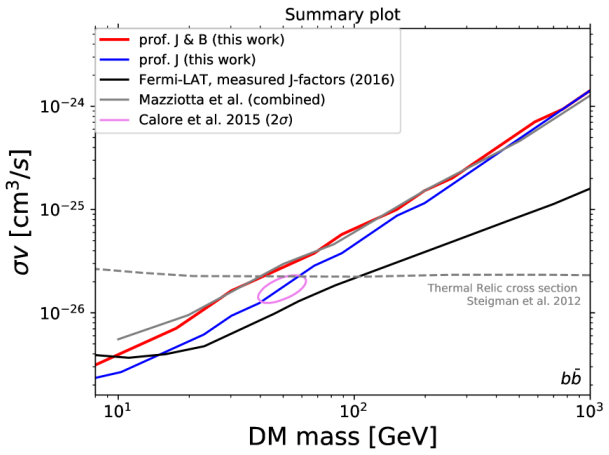

Figure 3: Comparison of current limits on the DM parameters: the main result of this work when profiling over J-factor (blue line) and also background uncertainties (red line), Fermi-LAT (black line), and other data-driven approaches (grey line). The purple contour represents the 2σ best-fit region.

erning the background. Once we have estimated the expected number of gamma-ray counts from the background in this way, a traditional procedure is followed to compare it with the observations at the different dSph galaxies, in order to make a statistical statement about the DM emission.

A data-driven model of the background emission

Traditional Machine Learning (ML) models assume a parametric probability distribution (likelihood) of the observables y. For example, in the case of real variables, a common assumption is a Gaussian likelihood, $y(\mathbf{x}) \sim \mathcal{N}(\mu(\mathbf{x};\theta),\sigma)$, with mean $\mu(\mathbf{x};\theta)$ given by some non-linear function (e.g. a neural network) with parameters θ, and a d-dimensional input $\mathbf{x}$. However, in many situations the Gaussian assumption is not justified, and may give poor predictive performances. We follow instead another ML approach, concerning the so-called " non-parametric" models, giving a likelihood function whose expressivity increases with the number of data points considered. Concretely, we write the joint likelihood $p(\mathbf{x}, y)$ as:

$$p(\mathbf{x}, y) = \frac{1}{N}\sum_{i=1}^{N} k_\sigma(\mathbf{x}-\mathbf{x}_i) g_\varsigma(y-y_i) \ , \qquad (1)$$

where the index i runs over all the N available data points, while $k_\sigma(\cdot)$ and $g_\varsigma(\cdot)$ are kernel functions with parameters σ and ς respectively. For our particular problem, $\mathbf{x}$ represent the vector of galactic longitude and latitude, while the observable y represents the number of photons measured by Fermi-LAT. Under very weak hypotheses of continuity and smoothness, Eq. (1) is guaranteed to provide an unbiased estimator for the true (but unknown) underlying likelihood. The above joint likelihood $p(\mathbf{x}, y)$ provide us a way to estimate the expected value $\lambda_{\rm bckg}(\mathbf{x})$ of the observable as:

$$\lambda_{\rm bckg}(\mathbf{x}) \equiv \mathbb{E}_{p(y|\mathbf{x})}[y] = \frac{\sum_{i=1}^{N} k_\sigma(\mathbf{x}-\mathbf{x}_i) y_i}{\sum_{i=1}^{N} k_\sigma(\mathbf{x}-\mathbf{x}_i)} \ . \qquad (2)$$

In order to make predictions, we first need to fix the model parameters σ, ς. In this work we follow a Maximum Likelihood Estimate procedure, where we choose the parameters that maximise the global log-likelihood of the whole data.

Bounds on the dark matter interactions

The expected background emission predicted with the above procedure should be added to the expected emission coming from the (hypothetical) DM interactions with the photons. We choose a typical WIMP dark matter, and for concreteness, focus on the case where these particles self-annihilate directly to bottom quarks, which subsequently decay and produce a spectrum of gamma-ray photons. The expected number of photons coming from DM annihilation at a given dwarf galaxy d can be expressed as:

$$\lambda_{\rm DM} = J_d \langle\sigma v\rangle f(m_{\rm DM}) \ , \qquad (3)$$

where J_d encodes the DM content (actually, its integral along the line-of-sight) at the dSph d, $\langle\sigma v\rangle$ is the velocity-averaged DM annihilation cross section, and the function $f(\cdot)$, depending on the DM mass $m_{\rm DM}$, encodes the spectral information of the DM annihilation.

As customary in the literature, we are interested in extracting bounds on the DM annihilation, for which we follow a frequentist approach. Fig. 3 shows a summary of our results. The solid lines represent the upper bound on $\langle\sigma v\rangle$ as a function of the DM mass. The most statistically complete result corresponds to the red curve, where we have in a way marginalised over the background contributions, something that was not possible so far in the literature. Comparing with the official results from Fermi-LAT (see black curve) we realise that our bounds on DM turn out to be more conservative, which is the result of taking into account the background uncertainties (unlike the Fermi result).

Concluding remarks

A proper data-driven inclusion of background uncertainties in the derivation of DM upper limits is not only possible, but very much needed for a fair comparison with limits from other targets, where theoretical background uncertainties are traditionally more explored than in dSphs analyses.

Notes

a. Email: b.zaldivar.m@csic.es

References

[1] F. Calore, P. D. Serpico and B. Zaldivar, *JCAP* ***10*** *(2018), 029 [arXiv:1803.05508 [astro-ph.HE]].*

Modeling of properties and phase transformations at high temperatures of 2.25Cr-1Mo steels

Yuniel Ernesto Martínez Pérez[a1], René Collazo Carceller[1], Miguel Armando Autie Pérez[1], and José Luis Valín-Rivera[2]

[1]Faculty of Mechanical Engineering, Technological University of Havana José Antonio Echeverría, Havana, Cuba
[2]School of Mechanical Engineering, Pontifical Catholic University of Valparaíso. Quilpué, Chile

The aim of this work was to analyse the values of thermo-physical and thermo-dependent mechanical properties and diagrams necessary at high temperatures for the simulation of a welding process of 2.25Cr-1Mo steels based on the compositions provided in the specialised literature.[b]

Welding is one of the most widely used joining methods for fastening elements. Simulation of welding processes is widely accepted as an important tool for the analysis of the evolution and interrelation of temperature, stress and strain fields in welded structures, as well as the evolution of the microstructure and distortion present. One of the complications that exist in welding simulation is that the necessary thermo-physical and thermo-dependent mechanical properties have been determined for a small number of specific alloys. On the other hand, the information is sometimes incomplete as not all the required properties are measured and generally scattered information from various sources is used to build up a database of the alloy used. In addition, this scattered information differs from one author to another. The main objective of the present work is to analyse the values of thermo-physical and thermo-dependent mechanical properties and diagrams necessary at high temperatures for the simulation of a welding process of 2.25Cr-1Mo steels based on the compositions given in the specialised literature.

Materials and Methods

The samples of compositions used (SC) during the study, all with nominal designation 2.25Cr-1Mo, are presented. The method used to obtain the thermo-physical and thermo-dependent mechanical properties was that of modelling using software that allows this type of study to be carried out depending on the composition of the material. The models by means of which the aforementioned properties and diagrams were obtained are also presented. See Table 1

S	C	Mn	P	S	Si	Cr
C1	0.15	0.6	0,03	0,03	0,5	2,6
C2	0,050	0,3	0,03	0,03	0,5	1,9
C3	0,102	0,433	0,014	0,0048	0,31	2.09
C4	0,1176	0,4	0.015	0.0136	0.31	2.50

S	Mo	Cu	Al	Ni	V
C1	1,13	x	x	x	x
C2	0,87	x	x	x	x
C3	0,93	0,12	0,02	0,03	0,011
C4	1.12	x	x	x	x

Table 1: Compositions of 2.25Cr-1Mo steel (wt %) studied.

Results and Discussion

The presence of ferrite at room temperature, its transformation into austenite and the carbides present are consistent with experimental reference results (Dèpinoy et al. [2]). Carbide M23C6 was found to dissolve in the intercritical temperature range (except for C2) with C1 being the composition that gives the best approximations. In contrast, M6C stabilises, for C1, C2, C3 and C4, at a temperature of 722°C, 730°C, 750°C and 660°C. The observed difference is due to the variation in the concentrations of the compositional chemical elements in each of the compositions studied. See Fig. 1.

The MnS particles were present in small concentrations, although they are higher and stabilise at higher temperatures than those described in the literature, except for C3, which stabilises at 1250°C. Although this behaviour of MnS is reported for steels such as the one studied, no work has been found so far that shows a similar behaviour for the compositions analysed in this study.

Figure 2 shows that the TTT diagrams obtained present a similar and coherent behaviour to those presented in the specialised literature. The differences are due both to the chemical composition and to the different austenitisation processes used, where these determine the grain size of the material, there being a strong dependence in obtaining these TTT diagrams with respect to the grain size.

The specific heat increases up to temperatures around 720°C, coinciding with the decrease of carbide type M6C. From 720 to 880°C it starts to decrease. There is a zone where the decrease is very small and appears to be practically constant. This is due to the transformation from ferrite to austenite between 800°C, when the first austenite grains begin to appear, and 860°C, when all the ferrite became austenite.

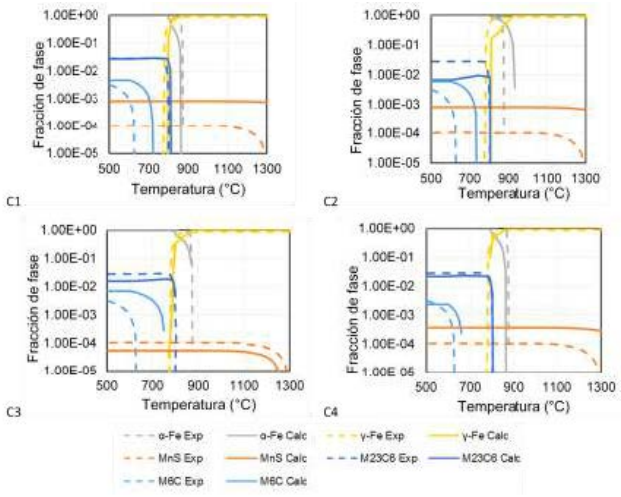

Figure 1: Comparison of the phase equilibrium diagrams obtained (solid lines) and those presented by Dépinoy et al. [2](dashed lines).

From this point onwards, the decrease in specific heat values is more noticeable. From 880°C onwards, its behaviour changes again and it starts to rise since the phase present is already austenite, with the presence of MnS.

As for thermal conductivity, the values obtained for the four compositions shown that at temperatures above 820°C contrasts with the values reported by the specialized literature. This is due to the difference between the chemical compositions and the heat treatment of the steels studied (including those reported by the reference). On the other hand, figure 4b shows which groups show significant differences. From 300°C to 820°C, a decrease in thermal conductivity as a function of temperature is observed. Coinciding with AC3, after 820°C there is a tendency for this property to increase.

The obtained behaviour of the density tends to decrease with increasing temperature and up to 800°C is similar to that suggested by the reference literature. The differences at temperatures above 800°C are a consequence of the variability of the chemical composition and the austenitisation heat treatment to which the steels were subjected. The observed jump coincides with the temperature range in which the ferritic-austenitic transformation of the material occurs and with the presence of M23C6 carbide.

In the case of thermal expansion, from 800°C the thermal expansion decreases due to the transformation of ferrite into austenite. From 870°C to 1430°C it rises linearly due to the completed transformation and the dissolution of carbides in the austenite. From 1430 ºC the dissolved carbides start to diffuse until 1530°C where the austenite can be considered homogeneous.

In all cases, it can be seen that Young's modulus decreases with increasing temperature. It can be seen that there are differences between the behaviours suggested by the literature consulted. The behaviours obtained in the present work by means of the modelling

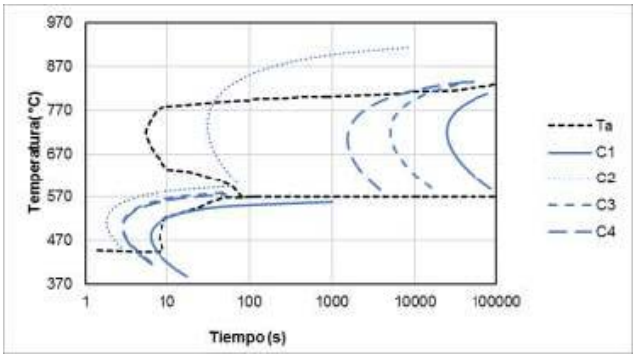

Figure 2: TTT diagrams for steels with denomination 2.25Cr-1Mo compared with those presented by Tsai et al. [3]

differ graphically from those presented in the works already referred to. This is more evident at temperatures above 820°C. A tendency for the Poisson's coefficient to increase with increasing temperature was found, which is in line with results from the literature.

Conclusions

The thermo-dependent properties and the high temperature diagrams necessary for the simulation of a welding process of a 2.25Cr-1Mo steel obtained by modelling are in correspondence with those reported in the specialised literature. The austenitisation treatment, the chemical composition and the carbides present significantly influence the behaviour of the thermo-dependent properties and diagrams obtained in the present work. The thermo-dependent behaviour at high temperatures of the thermo-physical and mechanical properties and phases described in the simulation of a welding process of a 2.25Cr-1Mo steel must be taken into account.

Notes

a. Email: yunimape@gmail.com

b. Original version of this article is in Ref [1]

References

[1] Martínez-Pérez, Y. E., Collazo-Carceller, R., Autie-Pérez, M. A.and Valín-Rivera, J. L., Modelación de propiedades y transformaciones de fase a altas temperaturas de aceros 2.25Cr-1Mo, *Ingeniería Mecánica,* **24** 1 (2021) 46-54.

[2] Dépinoy, S., Toffolon-Masclet, C., Urvoy, S. et al., Carbide Precipitation in 2.25 Cr-1 Mo Bainitic Steel: Effect of Heating and Isothermal Tempering Conditions, *Metall Mater Trans A,* **48** (2017) 2164-2178.

[3] Tsai, M. C., Chiou, C. S and Yang, J. R., Microstructural evolution of simulated heat-affected zone in modified 2.25Cr-1Mo steel during high temperature exposure., *Journal of Materials Science,* **38** (2003) 2373-2391.

Rapid crystallization enables controlled and highly stable hybrid perovskite phase transition

Sandy Sanchez [a1]

[1]Laboratory of Photomolecular Sciences, Institute of Chemistry and Chemical Engineering, 1015 Lausanne, École Polytechnique Fédérale de Lausanne, Switzerland

Perovskite hybrid semiconductor materials have an enormous potential for growth across the field with promising applications such as thin-film solar cells. Although device stability is the bottleneck of perovskite solar cell technology, recent advances show a promising way to implement future improvements.

In the field of hybrid perovskite materials, processing methods, compositional engineering, and other approaches need further development to compete with the most stable PV devices, such as silicon solar cells. However, scaling up perovskite solar cells (PSCs) for industrial production is a complex task for this young technology, mainly due to the poor stability of the material. Numerous approaches have been proposed to overcome this problem, and the different strategies can be divided into three categories: 1- chemical passivation; 2- compositional engineering; and 3- new synthesis methods.

The three mentioned strategies focus on removing crystal defects, either from the bulk or from the surface. The selecting layers and the final chosen architecture are also part of the problem to be solved; however, the perovskite attracts the most attention and is also the fundamental component of the cell.

A defect-tolerant perovskite film is less likely to be degraded from interstitial defects and deep traps, causing non-radiative centers, which are significantly related to the crystallization mechanism. Defects can determine the microstrain change in the perovskite lattice during crystal nucleation and growth, which can be further detrimental by external stress factors like humidity, photodegradation, and temperature. These defects will directly affect ion migration, non-radiative recombination, and organic decomposition, which are examples of mechanisms triggering irreversible degradation pathways.

Rapid IR hybrid perovskite crystallization

When a coated wet perovskite film is annealed, the heat provided by an IR pulse is the driving force to reach the supersaturation state by rapidly decreasing the concentration, thereby initiating nucleation and crystal growth. Looking at the specific FIRA case, crystal nucleation and growth can be controlled by the chamber temperature, pulse duration, and pulse number, as shown in Fig. 1a. Once nucleation has occurred, it is followed by the growth of a crystalline phase. The perovskite crystal formation can involve numerous intermediate phases that the growth rate can determine. The highly intense IR pulse causes the rapid evaporation of the solvent and provides the required thermal

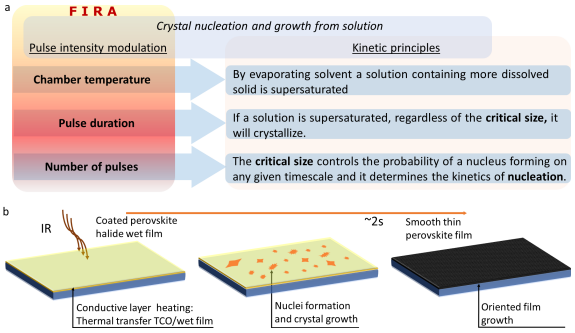

Figure 1: Schematic of the kinetic process in the nucleation and growth of a crystalline perovskite film from a solution and a) its relationship with the IR photonic pulses system, b) the sequential thin film perovskite formation.

activation energy for crystal nucleation and growth [1]. Interestingly, the IR pulse heats the conductive contact, rapidly transferring the thermal energy through the solid/liquid interface, as shown in Fig. 1b, where the thermal diffusion and interfacial energy lead to crystal growth. Then, by adjusting the number of pulses, the heating rate controls how supersaturation is reached and, as a consequence, how the nuclei distribution from tiny clusters defines the final crystal shape.

The experimental investigation of crystal nucleation and growth is complex and challenging for almost all systems. The classical nucleation theory stipulates that the critical nucleus is a sphere. The essential factor is how the total free energy associated with forming an average critical nucleus depends on its size, whatever the shape. However, this is a steady or quasi-steady-state assumption. This analysis cannot apply to non-thermodynamic equilibrium when the temperature changes too fast, as in the case of the FIRA, which is still one of the main challenges for the rate calculations in these processes.

Quasi-infinity steady-state numeric calculations corresponding to non-isothermal conditions must be performed with a non-constant temperature rate. Particularly in perovskite film processing, the calculation of nucleation and growth rates needs to be adapted for specific cases.

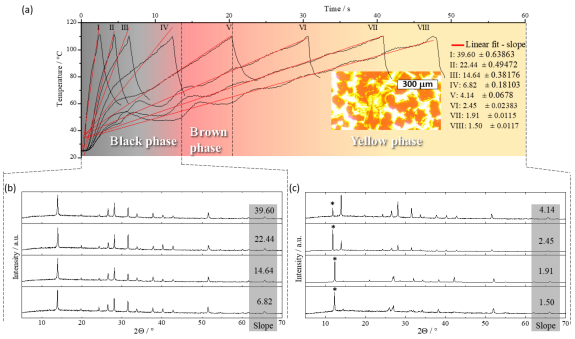

Figure 2: a) Temperature profile of the studied films under different heating rates with their respective linear fitting. Inset: optical image of a film processed with the lowest heating rate. b) and c) X-ray diffraction patterns of the selected films labeled with the respective heating rate-slope. The asterisk over the peaks highlight the δ phase.

The $FAPbI_3$ case

A phase transformation occurs during heating and cooling at specific temperatures, accompanied by enthalpic and entropic thermodynamic changes. Phase transitions can emerge via different kinetics pathways, for example, when applying rapid thermal annealing and quenching processes at different rates. Accordingly, to the published work [2] it was applied 17 pulse times and respective intensities to the spin-coated $FAPbI_3$ wet films with the IR photonic annealing method.

The IR pulse incident on the film has an estimated power density of 58.3 W/cm2, and rapid cooling was ensured by opening the annealing chamber after light pulsing. A temperature profile of 8 selected annealed films and their respective phase transitions as a function of the heating rates is shown in Fig. 2a. Note that the temperature evolution was measured on the film's surface with an IR pyrometer, and we used the slope of the curve until quenching as a reference for all heating rates for simplification. We identified three main regimes at this step, from black perovskite and mixed brown phases to the yellow non-perovskite phases, denoting the enthalpic and entropic effect on phase transition. The inset of Fig. 2a, indicates an inhomogeneous yellow $FAPbI_3$ film processed with the lowest heating rate.

The structural phases of the processed films have been characterized with x-ray diffraction (XRD) as shown in Figures 1b and c, XRD patterns of the perovskite and non-perovskite regimes, respectively. The patterns of the black phase regime evidence the absence of both PbI2 and other impurities.

$FAPbI_3$ has been reported as cubic by neutron diffraction at room temperature. Still, many other authors have claimed an alpha cubic phase by XRD characterization without an in-depth structural and symmetry analysis. In geometrical terms, the Pm-3m–I4/mcm phase transition has been widely observed in oxide perovskite materials, such as SrTiO3, due to lattice instabilities as in perovskite halides where strain can accumulate in the lattice upon substrate cooling.

For the $FAPbI_3$ IR annealed case, the used refinement model does not accurately match the cubic phase to our processed black films (in terms of peak positions); instead, a tetragonal, primitive unit cell matched the peak position the best. Besides, a small octahedral tilting at room temperature can produce a noncubic structure. Therefore, IR annealing crystallizes a black perovskite photoactive phase (which fits with a tetragonal state) instead of a cubic alpha phase. The nature of this structural phase and its symmetry-related aspects are a strong motivation for further work.

Notes

a. Email: sandy.sanchezalonso@epfl.ch

References

[1] S. Sánchez, L. Pfeifer, N. Vlachopoulos, and A. Hagfeldt, Rapid hybrid perovskite film crystallization from solution, *Chem. Soc. Rev.,* **50** (2021) 7108-7131

[2] S. Sánchez, S. Cacovich, G. Vidon, J. Guillemoles, F. Eickemeyer, S. M. Zakeeruddin, J. E. K. Schawe, J. F. Löffler, C. Cayron, P. Schouwink and M. Graetzel, Thermally controlled growth of photoactive $FAPbI_3$ films for highly stable perovskite solar cellse, *Energy Environ. Sci.,* **15** (2022) 3862